

LaTiO₂N/In₂O₃ photoanodes with improved performance for solar water splitting

Céline M. Leroy,^{*a} Alexandra E. Maegli,^b Kevin Sivula,^a Takashi Hisatomi,^a Nicolas Xanthopoulos,^c Eugenio H. Otal,^b Songhak Yoon,^b Anke Weidenkaff,^b Rosendo Sanjines^d and Michaël Grätzel^a

^aLaboratory of Photonics and Interfaces (LPI), Ecole Polytechnique Fédérale de Lausanne (EPFL), 1015 Lausanne, Switzerland

^bLaboratory for Solid State Chemistry and Catalysis, Empa - Swiss Federal Laboratories for Materials Science and Technology, 8600 Dübendorf, Switzerland

^cInterdisciplinary Centre for Electron Microscopy (CIME), Ecole Polytechnique Fédérale de Lausanne (EPFL), 1015 Lausanne, Switzerland

^dInstitute of Condensed Matter Physics, Ecole Polytechnique Fédérale de Lausanne (EPFL), 1015 Lausanne, Switzerland

Supporting information

1. Additional experimental details

To prepare the electrodes for this work, LaTiO₂N powder was first synthesized by heating La₂Ti₂O₇ powder at 1223 K for 16 h under a 200 mL.min⁻¹ NH₃ flow rate. The oxynitride photoanodes were next prepared by electrophoretic deposition on FTO substrates, followed by a post-necking treatment consisting in 5 dips with a methanolic solution of TiCl₄ (40 mM). The photoanodes were subsequently annealed at 773 K under a 2×10⁻⁵ mbar vacuum for 30 min.

The In₂O₃ layer was deposited by RF sputtering at room temperature, under a total Ar pressure of 1×10⁻² mbar and using a 5 cm-diameter In₂O₃ target. The deposition was performed for 50 s at a RF power of 100 W.

The thickness of the LaTiO₂N porous layer was measured with a Tencor Alpha-Step 500 profilometer. The thickness of the In₂O₃ layer was evaluated using a Sopra GES 5E spectroscopic ellipsometer and using an In₂O₃ reference deposited on Si substrates under the same sputtering conditions as the LaTiO₂N/In₂O₃ electrodes.

X-Ray diffraction (XRD) patterns were collected with a Bruker D8 Advance diffractometer operating , with Cu K_α radiation (filtered by a Ni β-filter) and a linear “lynx eye” detector. The diffractometer was operating in Bragg-Brentano geometry to investigate the crystallinity of the LaTiO₂N layer and in grazing incidence geometry at an angle of 6° to investigate the crystallinity of the In₂O₃ overlayer.

Transmission spectra were recorded using a Hewlett-Packard 8453 UV-Vis spectrophotometer.

The presence of the In₂O₃ layer was confirmed by performing Auger Electron Spectroscopy (AES), using a Perkin-Elmer PHI 660 Scanning Auger Microprobe in the Surface Analysis Facility of the Interdisciplinary Centre for Electron Microscopy (CIME) at EPFL. Primary electron beam potential and current were 5 kV and 10 nA, respectively. Depth profiling was performed using 2 keV argon ions and the sputtering rate was 4.5 nm.min⁻¹ as calibrated with a Ta₂O₅ NPL standard.

As AES tends to underestimate the content of light elements such as nitrogen and oxygen, the composition of the In₂O₃ layer was also assessed by X-ray photoelectron spectroscopy (XPS) using an Axis Ultra instrument (Kratos analytical, Manchester, UK) under ultra-high vacuum condition (<10⁻⁸ Torr) and using a monochromatic Al K_α X-ray source (1486.6 eV), also in the Surface Analysis Facility of the CIME. The source power was maintained at 150 W and the emitted photoelectrons were sampled from a square area of 750×300 μm². The photoelectron take-off angle, between the surface and the direction in which the photoelectrons were analyzed, was 90°. The analyzer pass energy was 80 eV for survey spectra and 40 eV for high-resolution spectra. Both curve fitting of the spectra and quantification were performed with the CasaXPS software, using relative sensitivity factors given by Kratos. The carbon 1s peak was calibrated at 285 eV and used as an internal standard to compensate for any charging effects.

Photocurrent measurements were performed under front-side chopped irradiation and in a three-electrode configuration using a 0.1 M Na₂SO₄ aqueous solution (pH 7) as the electrolyte, a Pt wire as the counter electrode, and an Ag/AgCl electrode in saturated KCl solution as the reference electrode.

The light source was simulated sunlight from a 450 W Xe-lamp (Osram, ozone free) passed through a KG3 filter (3 mm, Schott) with a measured intensity equivalent to standard AM1.5 sunlight ($100 \text{ mW}\cdot\text{cm}^{-2}$, spectrally corrected). As for the measurements reported in the literature for oxynitride photoelectrodes, no buffer has been used. This was not necessary as revealed by the stability of the pH measured before and after the photocurrent measurements and since, in any case, any effect of local pH change could be considered to be negligible given the relatively small photocurrents observed.

Chronoamperometry measurements were performed in the same conditions at 1.23 V vs. RHE. Due to the lack of perfect synchronization between the light chopping (performed with an externally controlled shutter) and the data acquisition, the precise time delay between the illumination switching and the following data point capture could not be controlled. This caused the observed transient amplitudes to erroneously appear to vary sinusoidally with time.

Photocatalytic reaction was carried out under irradiation of a 150 W halogen lamp (Osram, HLX 64640), in a 10 mM AgNO_3 solution (pH 8) containing 0.1 g of LaTiO_2N as the catalyst and 0.2 g of La_2O_3 as a pH buffer. A reaction vessel containing the reagents was connected to a vacuum pump and a gas chromatograph (HRGC 5300, Carlo Erba), which was equipped with MS-5A columns (60/80 mesh, length: 5 m, diameter: 3.1 mm, Restek), He carrier gas (99.999%, Carba gas) and a TCD detector (HWD 430, Carlo Erba) for gas separation and detection. After evacuation, the reactor was filled with 100 mbar of He and irradiated with the light source.

Photocurrent action spectra were obtained under light from a 300 W Xe-lamp with integrated parabolic reflector (Cermax PE 300 BUUV) passing through a monochromator (Bausch & Lomb, bandwidth 10 nm fwhm). The wavelength was scanned at $5 \text{ nm}\cdot\text{s}^{-1}$ and the monochromatic photocurrent of the electrodes compared with that of a UV enhanced Si-photodiode (Oriel 71883) of known IPCE spectrum. To discount the dark current in the IPCE measurement, the measurements were performed under light chopping conditions and the IPCEs points reported were obtained by subtracting the data points recorded in the dark to the one recorded under irradiation.

2. Additional data

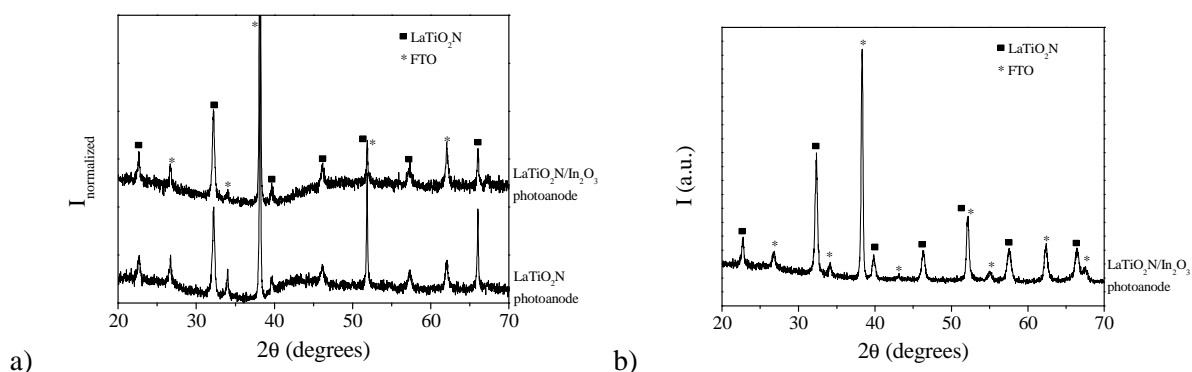


Fig. S1 a) XRD patterns of the LaTiO_2N and $\text{LaTiO}_2\text{N}/\text{In}_2\text{O}_3$ photoanodes collected in Bragg-Brentano geometry. The intensities have been normalized with regard to the most intense reflection of the FTO substrates. b) XRD pattern of the $\text{LaTiO}_2\text{N}/\text{In}_2\text{O}_3$ photoanode collected in grazing incidence geometry.

In all cases, the only other reflections than that of the FTO corresponded to the LaTiO_2N perovskite-type phase. The LaTiO_2N crystallinity appeared to be the same with and without the In_2O_3 layer. No reflection corresponding to any crystalline phase of TiO_2 , TiN , In_2O_3 , La_2O_3 or $\text{La}_2\text{Ti}_2\text{O}_7$ was visible. The In_2O_3 layer was likely amorphous considering (i) the absence of any In_2O_3 reflections on the diffractogram collected in grazing incidence geometry, (ii) the deposition method that generally results in amorphous materials when oxide layers of such thicknesses are deposited at room temperature, especially on the top of materials presenting a different crystalline structure, which is favorable to dead layer effects.

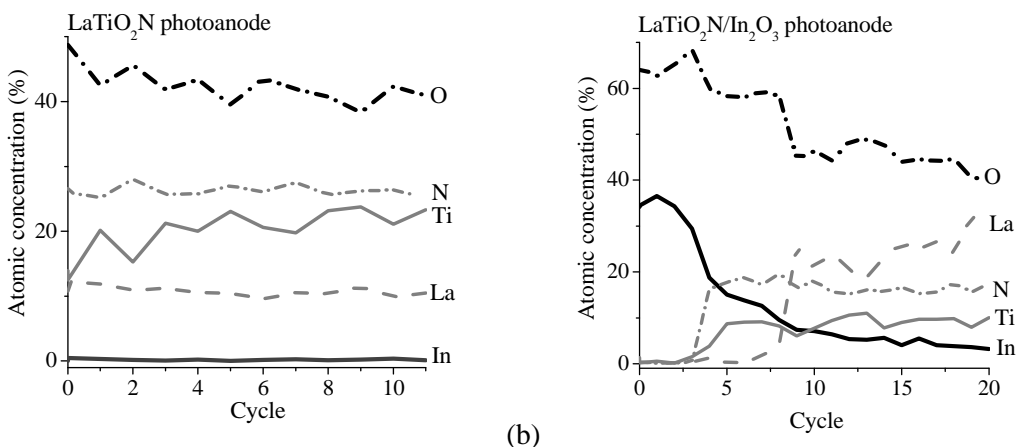


Fig. S2 AES depth profiles of the (a) LaTiO₂N and (b) LaTiO₂N/In₂O₃ photoanodes testifying to the successful deposition of the In₂O₃ overlayer. For the LaTiO₂N electrode (a), the In atomic concentration was zero and the atomic concentrations of the other elements were stable and consistent with the composition of the LaTiO₂N layer (despite a slight La understoichiometry). For the LaTiO₂N/In₂O₃ electrode (b), In and O were the only elements at the surface – with a ratio consistent with a In₂O₃ phase – and their concentrations progressively decreased during etching while the concentrations of the La, Ti and N progressively increased due to the transition from the In₂O₃ overlayer to the LaTiO₂N layer.

Table S1 Comparison of the XPS and theoretical chemical composition ratios of the In₂O₃ sputtered layers.

	XPS	Theoretical
In/(In+O) ratio (at. %)	42	40
O/(In+O) ratio (at. %)	58	60

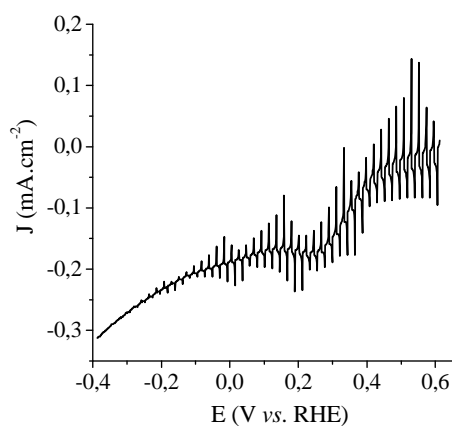


Fig. S3 Current density-voltage (J-V) curve of a LaTiO₂N photoanode in a 0.1 M Na₂SO₄ aqueous electrolyte and under a chopped AM1.5 irradiation. The scanning was performed toward cathodic potentials at a scan rate of 10 mV·s⁻¹.

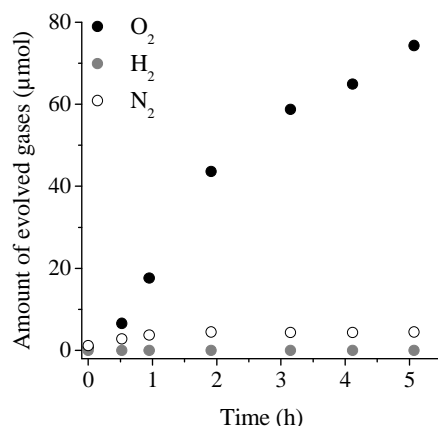


Fig. S4 Time course of photocatalytic gases evolution using LaTiO₂N photocatalyst (0.1 g) suspended in a 10 mM AgNO₃ aqueous solution (pH 8 buffered with 0.2 g of La₂O₃) under irradiation of a 150 W halogen lamp.

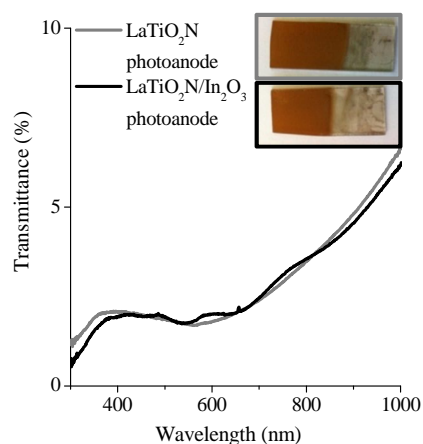


Fig. S5 Transmittance spectra and photographs of the LaTiO₂N and LaTiO₂N/In₂O₃ photoanodes.

Table S2 Comparison of the photocurrent densities at different applied potentials, before and after deposition of the In₂O₃ layer.

Applied potential E		0.75 V vs. RHE	1.23 V vs. RHE	1.45 V vs. RHE
Photocurrent density J (mA.cm ⁻²)	LaTiO ₂ N photoanode	0.13	0.24	0.36
	LaTiO ₂ N/In ₂ O ₃ photoanode	0.32	0.61	0.76
J variation through In ₂ O ₃ deposition		+ 157 % (× 2.7)	+ 154 % (× 2.5)	+ 113 % (× 2.1)

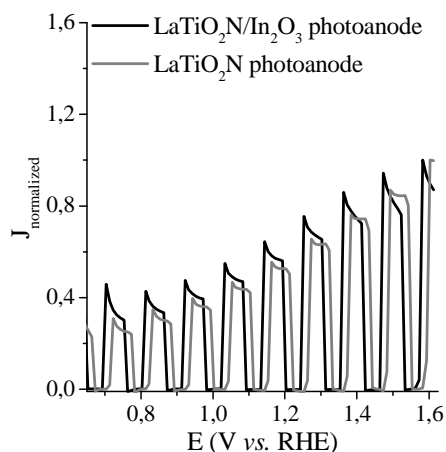


Fig. S6 Normalized current density-voltage (J - V) curves of the LaTiO₂N and LaTiO₂N/In₂O₃ photoanodes, in a 0.1 M Na₂SO₄ aqueous electrolyte and under a chopped AM1.5 irradiation (scan rate 10 mV.s⁻¹).

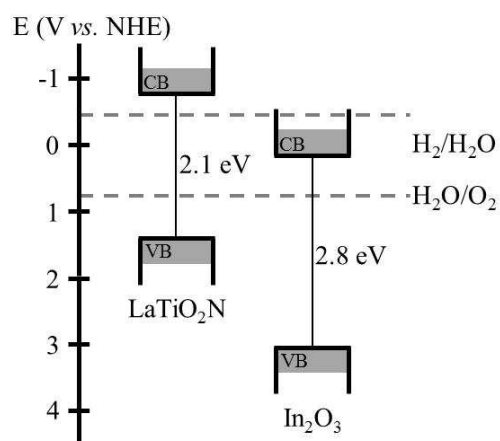


Fig. S7 Energy band diagram of LaTiO₂N and In₂O₃ at pH 7, extrapolated from literature data.^{1, 2}

3. References

1. C. Le Paven-Thivet, A. Ishikawa, A. Ziani, L. Le Gendre, M. Yoshida, J. Kubota, F. Tessier and K. Domen, *J. Phys. Chem. C*, 2009, **113**, 6156-6162.
2. A. Kudo and I. Mikami, *J. Chem. Soc., Faraday Trans.*, 1998, **94**, 2929-2932.